Earth and Planetary Science Letters 594 (2022) 117718

Contents lists available at ScienceDirect

Earth and Planetary Science Letters

www.elsevier.com/locate/epsl

Rapid preservation of Jehol Biota in Northeast China from high precision $^{40}Ar/^{39}Ar$ geochronology

Youjuan Li [a], Brian R. Jicha [a], Zhiqiang Yu [b], Huaichun Wu [c], Xiaolin Wang [d], Brad S. Singer [a], Huaiyu He [b,*], Zhonghe Zhou [d]

[a] Department of Geoscience, University of Wisconsin-Madison, 1215 West Dayton Street, Madison, WI 53706, USA
[b] State Key Laboratory of Lithospheric Evolution, Institute of Geology and Geophysics, Chinese Academy of Sciences, Beijing 100029, China
[c] State key Laboratory of Biogeology and Environmental Geology, China University of Geosciences, Beijing 100083, China
[d] Key Laboratory of Vertebrate Evolution and Human Origins of Chinese Academy of Sciences, Institute of Vertebrate Paleontology and Paleoanthropology, Chinese Academy of Sciences, Beijing 100044, China

ARTICLE INFO

Article history:
Received 14 February 2022
Received in revised form 8 June 2022
Accepted 4 July 2022
Available online 25 July 2022
Editor: B. Wing

Keywords:
Lujiatun
Jianshangou
Jehol Biota
$^{40}Ar/^{39}Ar$ dating
sedimentation
feathered dinosaur/primitive bird

ABSTRACT

In Liaoning Province, Northeastern China, the Early Cretaceous Jehol Biota records significant evolution and radiation of fauna in terms of diversity, abundance and complexity. The alluvial-to-fluvial Lujiatun and lacustrine Jianshangou beds of the lower Yixian Formation yield exceptionally well-preserved three-dimensional and articulated dinosaur and mammal fossils, and two-dimensional primitive birds/feathered dinosaurs, respectively. Published $^{40}Ar/^{39}Ar$ ages for the two fossil beds have uncertainties of ± 0.4 to 1.0 Ma (± 2σ analytical uncertainty), and these reflect the measurement of large, and potentially heterogeneous, populations of feldspar crystals. More precise constraints on the timing and duration of biological radiation recorded by this sequence can further quantify evolutionary patterns and rates of diversification of important Early Cretaceous animals and plants. Single crystal $^{40}Ar/^{39}Ar$ fusion experiments on sanidine from intercalated ash beds yield dates that constrain the deposition of the Jianshangou and Lujiatun fossil beds to between 125.374 ± 0.085 and 125.572 ± 0.120 Ma, and 125.541 ± 0.099 and 125.793 ± 0.127 Ma, respectively. These ages indicate that the lower part of Jianshangou fossil bed was deposited nearly contemporaneously with the Lujiatun fossil bed. Thus, mass mortality events reflected by dinosaur fossil concentrations in the Lujiatun fossil bed and feathered dinosaur/primitive bird fossils in the Jianshangou fossil bed were nearly coeval and short-lived. These $^{40}Ar/^{39}Ar$ ages, combined with astrochronologic and paleomagnetic results from the lacustrine sediments in the Jianshangou fossil bed, not only refine the duration and rapid radiation of primitive birds and feathered dinosaurs in the deposit, but also suggest that the distribution of magnetic polarity chron boundaries within the Barremian stage in the current geologic time scale (GTS 2020) requires a revision.

1. Introduction

The Early Cretaceous Jehol Biota reflects a center and cradle of diversification for many groups of animals and plants that were mainly distributed in the western part of Liaoning Province, northern Hebei Province, and southeastern Inner Mongolia in northeastern China (Manabe et al., 2000; Zhou et al., 2003; Zhou, 2006). It is a unique source for studying and comparing Early Cretaceous and modern terrestrial ecosystems (Zhou et al., 2003). The evolution history of Jehol radiation has been divided into early, middle, and late phases (Chen, 1988; Zhou, 2006). Many of the most significant and largest biological radiations occur during the middle phase and are preserved in sediments of the lower Yixian Formation in the western part of Liaoning Province. For example, vertebrate groups including feathered dinosaurs, early birds, pterosaurs, and mammals (Wang et al., 1998; Luo et al., 2003; Zhou, 2006), as well as invertebrate groups, such as insects, ostracods, and conchostracans (Zhang and Zhang, 2003), show initial and most expansive radiations during the middle phase. Similarly, the Jehol Flora, including early angiosperms, genetales, and sphenopsids, also display maxima in abundance and diversity, which is thought to be connected to the wider radiation of animal groups (e.g., Leng and Friis, 2003). It has been suggested that increased tectonic activity and frequent volcanic eruptions might have played an important role in the mass mortality and exceptional preservation of the animal and plant fossils (Jiang et al., 2014; Zhou and Wang, 2017).

* Corresponding author.
E-mail address: huaiyuhe@mail.iggcas.ac.cn (H. He).

https://doi.org/10.1016/j.epsl.2022.117718
0012-821X/

The Lujiatun and Jianshangou fossil beds are sedimentary horizons in the lower Yixian Formation, which are characterized by exceptionally high-quality preservation of Jehol fossils. The Lujiatun fossil bed is well-known for the occurrence of three-dimensional and articulated fossils of dinosaurs, mammals, anurans and lizards without any trace of soft-tissue, some of which preserved behavioral and anatomical information (Zhou, 2006). An adult ornithischian dinosaur *Psittacosaurus sp*., for instance, clustered with 34 juveniles, indicates the presence of post-hatching parental care among dinosaurs (Meng et al., 2004). The holotype of *Mei long*, a troodontid dinosaur, is preserved in the stereotypical sleeping (or resting) posture, providing compelling evidence for the dinosaurian origin of birds (Xu and Norell, 2004). A well-preserved herd of the ceratopsian dinosaur *Psittacosaurus* constitutes the first direct evidence for post-nestling gregarious social behavior (Zhao et al., 2007). A fossil preserving most of the skull, postcranium, and stomach contents represent the first direct evidence that large mammals fed on baby dinosaurs (Hu et al., 2005). The tuffs within the Lujiatun fossil bed are structureless and lack obvious bedding planes. In parallel with the three-dimensional vertebrate fossils, sedimentary analysis suggests that these deposits record a single, catastrophic mass mortality event (Wang and Zhou, 2003; Zhao et al., 2007; Jiang et al., 2014) or multiple, rapid, flood events with a high load of volcaniclastic debris (Rogers et al., 2015).

The Jianshangou fossil bed represents the most important horizon preserving 40 genera and species of vertebrates, including important primitive birds, feathered dinosaurs, pterosaurs and early mammals (Wang et al., 1998; Wang and Zhou, 2003; Jiang and Sha, 2007), including: theropoda dinosaurs: *Sinosauropteryx prima, Sinornithosaurus milleni, Beipiaosaurus inexpectus, Protachaeopteryx robusta, Caudipteryx zoui and C. dongi;* ceratopsian dinosaur *Psittacosaurus*; primitive birds of two genera and three species, *Confuciusornis sanctus, C. suniae, Liaoningornis longiditris*; pterosaurs of four genera and three species, *Haopterus gracilis*, *Gegepterus zhangae, Eosipterus yangi, Dendrorhynchoides curvidentatus* and three genera of primitive mammals, *Zhangheotherium quinquecuspidens, Jeholodens jenkinsi, Maotherium sinensis*; fishes, *Lycoptera sinensis, Peipiaosteus pani*. In addition to vertebrates, this bed is also rich in invertebrates, including insects, ostracods, gastropods, bivalves, as well as plants. The Jianshangou fossil bed comprises tuffaceous deposits within finely laminated shales and mudstones, that permit exceptional preservation of soft tissues and microstructures, such as skin impressions, stomach contents, integumentary feathers and fur, hair, wing veins and color patterns (Zhou et al., 2003; Zhang et al., 2010).

The biological radiation recorded by the Lujiatun and Jianshangou fossil beds offers an important opportunity for elucidating animal behavior and anatomy, the evolution of feathers and flight, and the origin, early evolution, and radiation of birds and mammals. Efforts to determine the timing of the radiation of the Jehol Biota are numerous (e.g., Swisher et al., 1999, 2002; Wang et al., 2001a,b; He et al., 2006; Yang et al., 2007; Zhu et al., 2007; Chang et al., 2009, 2017; Zhong et al., 2021). However, most of the radioisotopic age determinations are imprecise, potentially inaccurate, or do not span sufficient intervals of the stratigraphic sections to address important questions about the duration and pace of the biological radiations recorded by this sequence. Advances in $^{40}Ar/^{39}Ar$ geochronology (e.g., Schaen et al., 2021) are poised to improve the timeline of biological radiations and extinctions recorded by the Jehol Biota.

We present precise $^{40}Ar/^{39}Ar$ single sanidine fusion dates from seven tuffs within the Lujiatun and Jianshangou fossil beds that provide high resolution constraints on the time spanned by the two extraordinarily well-preserved fossil-bearing beds. The new $^{40}Ar/^{39}Ar$ dates span more of the salient stratigraphic sections than previous studies. Linked to an astronomical age model for the Jianshangou fossil bed (Wu et al., 2013), these dates offer new insights regarding the duration and rapid radiation of primitive bird, feathered dinosaurs and pterosaurs were preserved. Moreover, our findings suggest that the timing of normal magnetic polarity chron boundaries within the Barremian stage in GTS 2020 (Gale et al., 2020; Ogg, 2020) require modification.

2. Geological background and sampling

Various schemes of lithostratigraphic nomenclature are proposed for the lower Yixian Formation in western Liaoning Province (e.g., Wang et al., 1998; Wang and Zhou, 2003; Wang et al., 2016). We use the most widely accepted stratigraphic column of Wang and Zhou (2003), with the modification of Wang et al. (2016), that raises the rank of beds to members (Fig. 1C). From bottom to top are the Lujiatun, Lava, and Jianshangou members. The Lujiatun member is mainly composed of alluvial and fluvial volcanic-rich conglomerates, tuffaceous sandstones and tuffs. Three-dimensional, articulated vertebrate fossils are preserved in these tuffs, which are structureless, massive, and lack bedding planes. The succeeding lava member comprises basaltic and andesitic lavas with volcanic breccia. The overlying Jianshangou member mainly comprises light to dark gray shales, fine-grained sandstones, and silty mudstones with tuffaceous components that reflect a lacustrine environment. The Jianshangou member is further divided into five beds, labeled 5 through 9 (Fig. 1C). Bed 6 (Jianshangou fossil bed) is most notable for preserving feathered dinosaurs and primitive birds, including *Sinosauropteryx, Beipiaosaurus, Sinornithosaurus, Confuciusornis*, and *Liaoningornis*. The fossil-bearing layers in this sequence are finely laminated shales and mudstones interbedded with tuffs.

Sihetun and Lujiatun villages are important and classic fossil-preservation sites of the Jianshangou and Lujiatun members, respectively, both located about 24-25 km south of Beipiao city, Liaoning Province, China (Fig. 1B). The Lujiatun fossil site is located about 9 km east of the Sihetun fossil site. Seven tuff samples were collected for $^{40}Ar/^{39}Ar$ dating (Fig. 1). Five samples (SHT20-6, SHT17-1, SHT17-3, SHT17-4 and SHT20-1) are from the fossil-bearing bed 6 of Jianshangou member in the classic Sihetun 11-meter (11 m) section (41.58861° N, 120.792500° E). The thickness of samples SHT20-6, SHT17-1, SHT17-3 and SHT20-1 are 5, 15, 7-8, and 1 cm, respectively. Sample SHT17-1 is located about 1.8 m below SHT20-6, SHT17-4 is about 1.77 m below SHT17-3, and SHT20-1 is about 2.2 m below the SHT17-4 (Table 1). Many vertebrate fossils are found near the sampled tuffs SHT17-3, SHT17-4 and SHT20-1, with abundant feathered dinosaurs and primitive birds ~1.5 to 2.0 m below sample SHT17-4. Two samples LJT17-1 (41.602222° N, 120.913333° E) and LJT17-2 (41.602500° N, 120.912500° E) are from bed 1 of Lujiatun member (Lujiatun fossil bed) in Lujiatun village, with LJT17-2 below LJT17-1. The Lujiatun tuffs mainly preserved three-dimensional invertebrate fossils (Zhou, 2006).

3. $^{40}Ar/^{39}Ar$ methods

Sanidine crystals (150-300 μm) were packed in aluminum foil, alongside the Fish Canyon sanidine (FCs) standard, into 4 mm wells within a 2.5 cm diameter aluminum disk. Samples SHT20-1 and SHT20-6 were irradiated in the Cadmium-Lined-In Core-Irradiation Tube (CLICIT) for 50 hours at the Oregon State University reactor; the other five samples were irradiated for 80 hours. $^{40}Ar/^{39}Ar$ single-crystal total fusion analyses used a 60 W CO_2 laser in the WiscAr Laboratory at the University of Wisconsin–Madison. The extracted gas was cleaned on an SAES GP-50 getter for 60 s and a cryotrap at −125 °C for 30 s, and then analyzed in a Nu Instruments Noblesse multi-collector mass spectrometer. The analytical

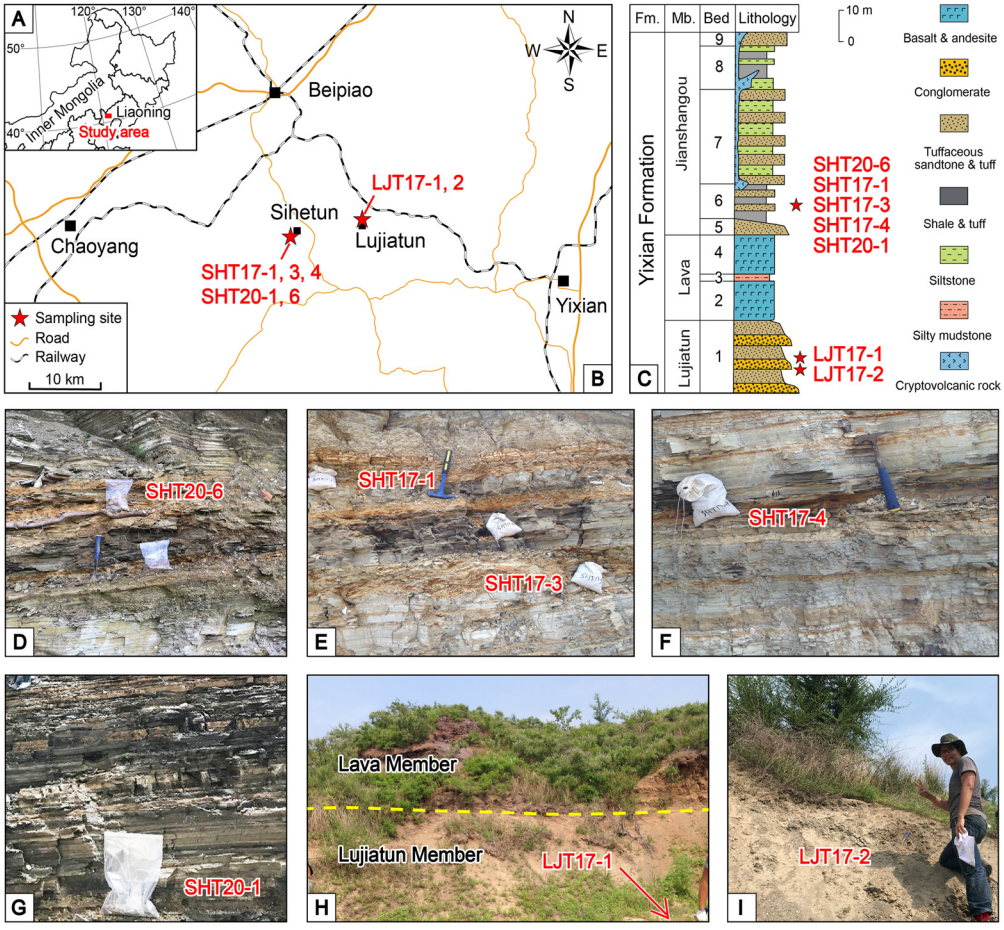

Fig. 1. (A) Location of the study area in northeast China. (B) Sample locations. (C) Traditional stratigraphic section of the lower Yixian Formation in Sihetun and the neighboring areas (modified from Wang and Zhou, 2003). (D-I) field photos. Fm—Formation; Mb—Member.

Table 1
Summary of $^{40}Ar/^{39}Ar$ single sanidine crystal age determinations from the Jianshangou and Lujiatun fossil beds.

Tuff sample	Depth in the 11 m Sihetun section (m)	Latitude (°N)	Longitude (°E)	*N*	MSWD	Wtd. mean age (Ma)	$\pm 2\sigma_{anal}$	$\pm 2\sigma_{int}$	$\pm 2\sigma_{ext}$
Jianshangou fossil bed									
SHT20-6	3.00	41.588611	120.792500	2 of 76	0.03	125.226	0.220	0.244	0.330
SHT17-1	4.80	41.588611	120.792500	34 of 35	0.75	125.374	0.050	0.085	0.240
SHT17-3	5.40	41.588611	120.792500	36 of 36	1.06	125.380	0.053	0.087	0.240
SHT17-4	7.17	41.588611	120.792500	29 of 32	0.85	125.414	0.051	0.086	0.240
Above three						125.389	0.029	0.049	0.136
SHT20-1	9.40	41.588611	120.792500	31 of 60	1.13	125.572	0.058	0.120	0.254
Lujiatun fossil bed									
LJT17-1	–	41.602222	120.913333	16 of 16	0.82	125.541	0.071	0.099	0.246
LJT17-2	–	41.602500	120.912500	5 of 11	0.39	125.793	0.106	0.127	0.258

Notes: All ages calculated relative to 28.201 Ma Fish Canyon Tuff sanidine standard (Kuiper et al., 2008), using decay constants of Min et al. (2000). Atmospheric $^{40}Ar/^{36}Ar$ = 298.56 ± 0.31 (Lee et al., 2006). N — number of single crystal fusion dates used for age calculation relative to the total number of dates. $\pm 2\sigma_{anal}$ — analytical uncertainty only at the 95% confidence interval. $\pm 2\sigma_{int}$ — analytical plus J uncertainty. $\pm 2\sigma_{ext}$ — fully propagated uncertainty at the 95% confidence interval including analytical, J value, standard age, and decay constant contributions.MSWD — mean square of weighted deviates; Wtd. mean age — Weighted mean age. Above three: SHT17-1, SHT17-3, SHT17-4.

procedure involves a sequence of repeated blank–cocktail gas–sanidine sample measurements (Jicha et al., 2016). Argon beam intensities were corrected for the blank, baseline, radioactive decay, and detector intercalibration, the latter of which was made using an in-house cocktail gas (Jicha et al., 2016). The $^{40}Ar/^{39}Ar$ ages are calculated relative to 28.201 ± 0.046 Ma Fish Canyon sanidine (FCs; Kuiper et al., 2008) using a $^{40}K_{total}$ decay constant of 5.463 × 10^{-10} yr^{-1} (Min et al., 2000) and an atmospheric $^{40}Ar/^{36}Ar$ ratio of 298.56 (Lee et al., 2006). Weighted mean $^{40}Ar/^{39}Ar$ ages are shown with uncertainties reported at the 95% confidence level in the form ± X(Y)[Z], where X is analytical uncertainty, Y combines analytical and J value (internal uncertainty), and Z combines analytical, J value, and decay constant and monitor mineral age uncertainties (external uncertainty).

4. Results

Samples SHT17-1, SHT17-3, and SHT17-4 from the Jianshangou fossil bed show excellent reproducibility with unimodal age distributions (Fig. 2). Thirty-four single-crystal total fusion sanidine analyses from SHT17-1 yield a weighted mean age of 125.374 ± 0.050(0.085)[0.240] Ma with a MSWD of 0.75 (Fig. 2B, Table 1). Thirty-six single-crystal fusions of SHT17-3 give a weighted mean $^{40}Ar/^{39}Ar$ age of 125.380 ± 0.053(0.087)[0.240] Ma (MSWD = 1.06,

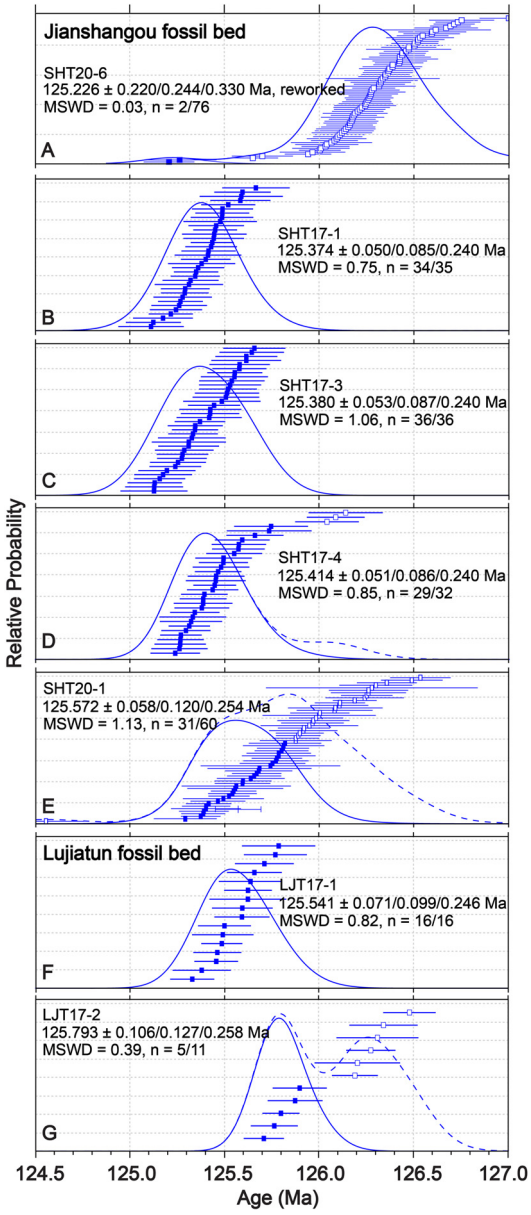

Fig. 2. Summary of $^{40}Ar/^{39}Ar$ dates from the Jianshangou and Lujiatun fossil beds. Open points denote analyses excluded from weighted mean age calculations. Weighted mean ages are shown with ± 2σ uncertainties (analytical/internal/external). MSWD—Mean Square of Weighted Deviates. The plots were created using Pychron software (Ross, 2019).

Fig. 2C, Table 1). For SHT17-4, 29 of 32 single-crystal sanidine fusions yield a weighted mean age of 125.414 ± 0.051(0.086)[0.240] Ma with a MSWD of 0.85 (Fig. 2D, Table 1). The youngest 31 of 60 dates from SHT20-1 give a weighted mean $^{40}Ar/^{39}Ar$ age of 125.572 ± 0.058(0.120)[0.254] Ma (one outlier excluded, MSWD = 1.13, Fig. 2E, Table 1). For SHT20-6, the youngest 2 of 76 single-crystal fusion analyses yield a weighted mean age of 125.226 ± 0.220(0.244)[0.330] Ma (MSWD = 0.03, Fig. 2A, Table 1).

Sixteen single-crystal total fusions from LJT17-1 from the Lujiatun fossil bed give a weighted mean age of 125.541 ± 0.071(0.099)[0.246] Ma (MSWD = 0.82, Fig. 2F, Table 1). The youngest 5 of 11 dates from LJT17-2 yield a weighted mean age of 125.793 ± 0.106(0.127)[0.258] Ma with a MSWD of 0.39 (Fig. 2G, Table 1). The above weighted mean ages are interpreted as the depositional ages. Complete $^{40}Ar/^{39}Ar$ isotope data are in supplementary Table S1.

5. Discussion

5.1. Timing of the Jianshangou and Lujiatun fossil beds

Samples SHT17-1, SHT17-3, and SHT17-4 from bed 6 of the Jianshangou fossil bed yield indistinguishable ages of 125.374 ± 0.050(0.085)[0.240], 125.380 ± 0.053(0.087)[0.240], and 125.414 ± 0.051(0.086)[0.240] Ma (Table 1). Thus, a weighted mean age of 125.389 ± 0.029(0.049)[0.136] Ma may be estimated for these three tuffs. Samples SHT20-1 and SHT20-6 each yield two age populations. Populations of $^{40}Ar/^{39}Ar$ sanidine dates that contain tails including dates older than the time of deposition (i.e., age dispersion) are common. Older dates have been interpreted to reflect: (1) xenocrysts derived from wall rock or underlying tuffs (e.g., Deino and Potts, 1990), (2) excess Ar within crystals (e.g., Ellis et al., 2017), or (3) antecrysts that grew detectably earlier than eruption of a magma (e.g., Andersen et al., 2017). Thus, the youngest portion of such a population most likely represents the age of eruption and deposition of a tuff. The weighted mean filter of Schaen et al. (2021) was used to determine the youngest population of $^{40}Ar/^{39}Ar$ dates for each sample. For sample SHT20-6, only two crystals yield dates that are younger than the dates from the underlying tuffs, such that the vast majority of the 76 crystals measured reflect reworking of underlying deposits. The youngest two crystals give a weighted mean of 125.226 ± 0.220(0.244)[0.330] Ma. The youngest population for sample SHT20-1 gives weighted mean age of 125.572 ± 0.058(0.120)[0.254], which we interpret to be the time since deposition. Thus, the five $^{40}Ar/^{39}Ar$ ages narrowly constrain the well-preserved fossiliferous Jianshangou fossil bed. Specifically, the $^{40}Ar/^{39}Ar$ age of 125.572 ± 0.058(0.120)[0.254] Ma for sample SHT20-1, that crops out only 0.2 to 0.7 m below the feathered dinosaur and primitive bird fossils of *Confuciusornis*, *Sinosauropteryx*, *Psittacosaurus sp.*, *Lycoptera sp.*, provides a precise age for these fossils.

For the Lujiatun fossil bed, two populations are obtained for sample LJT17-2, the older 6 crystals likely reflect reworking or xenocrystic contamination, with the youngest 5 dates producing a weighted mean age of 125.793 ± 0.106(0.127)[0.258] Ma. Sixteen crystals yield a weighted mean age of 125.541 ± 0.071(0.099)[0.246] Ma for sample LJT17-1. Unlike Jianshangou fossil bed with finely laminated sediments interbedded with tuff layers and two-dimensional compression fossils, the tuffs in Lujiatun fossil bed are massive and structureless, and preserve three-dimensional and articulated dinosaurs, lizards and mammals with behavior and anatomical information (Zhou, 2006). The Lujiatun fossil bed has been referred to as the "Chinese Pompeii" (Jiang et al., 2014). However, the nature of the mass mortality event and the exceptional preservation mechanisms of the fossils remain controversial. It has been proposed that the vertebrates were killed and buried by a single catastrophic pyroclastic flow or lahar (Wang and Zhou, 2003; Zhao et al., 2007; Jiang et al., 2014). Alternatively, Meng et al. (2004) suggest volcanic debris, entrapment in a collapsed burrow, or a flooding event, whereas Rogers et al. (2015) infer that multiple flood events with a high load of volcaniclastic debris buried and preserved these fauna. New $^{40}Ar/^{39}Ar$ ages of 125.541 ± 0.071(0.099)[0.246] and 125.793 ± 0.106(0.127)[0.258] Ma precisely date the deposition and preservation of these fossils.

Geochronologic findings from the Jianshangou and Lujiatun fossil beds are summarized in Fig. 3 and Table 2. Despite yielding many $^{40}Ar/^{39}Ar$ and U-Pb ages, stratigraphic correlation of the two fossil-rich beds has yet to be resolved. When comparing $^{40}Ar/^{39}Ar$ and U-Pb results, it is essential to use the full external uncertainties. The published $^{40}Ar/^{39}Ar$ ages were obtained from sanidine or groundmass, but in some cases used several to tens of milligrams of K-feldspar and employed a bulk incremental-heating method. The resulting age determinations could therefore be biased by in-

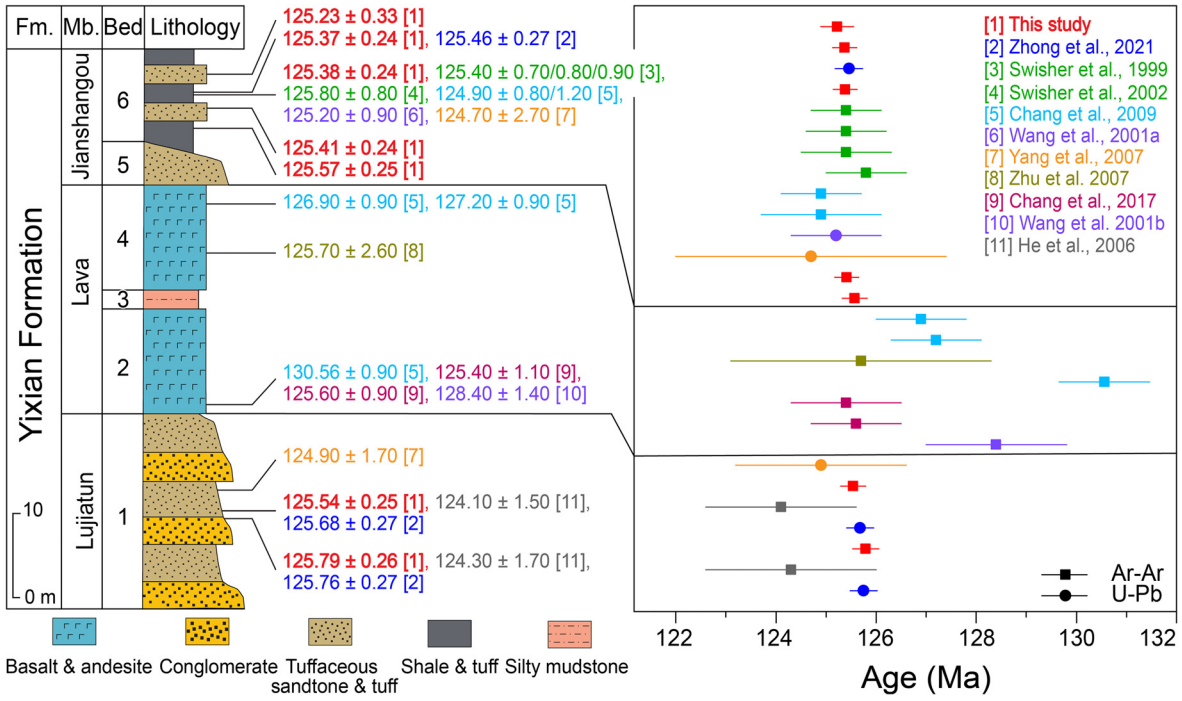

Fig. 3. Comparison of published $^{40}Ar/^{39}Ar$ and U-Pb ages for the lower Yixian Formation, and sampling positions. All data in this figure are from Table 2 with 2σ external uncertainties. The $^{40}Ar/^{39}Ar$ ages are recalculated relative to 28.201 Ma for the Fish Canyon sanidine (Kuiper et al., 2008) and decay constants of Min et al. (2000). *Notes*: 125.4 ± 0.7/0.8/0.9 from Swisher et al. (1999) represent 3 dates, 125.4 ± 0.7, 125.4 ± 0.8, and 125.4 ± 0.9 Ma.

Table 2
Summary of ages determined for the lower Yixian Formation.

Sample	Method	Material	Age (Ma) ± $2\sigma_{ext}$	References	Rock type and correlation
Jianshangou fossil bed					
P4T-1	$^{40}Ar/^{39}Ar$ incremental-heating	sanidine	125.4 ± 0.7	Swisher et al., 1999	same as SHT17-3
P4T-1	$^{40}Ar/^{39}Ar$ SCLF	sanidine	125.4 ± 0.8	Swisher et al., 1999	same as SHT17-3
P1T-2	$^{40}Ar/^{39}Ar$ SCLF	sanidine	125.4 ± 0.9	Swisher et al., 1999	same as SHT17-3
99L-S1	$^{40}Ar/^{39}Ar$ SCLF	sanidine	125.8 ± 0.8	Swisher et at., 2002	same as SHT17-3
YX07-4	$^{40}Ar/^{39}Ar$ incremental-heating	sanidine	124.9 ± 0.8	Chang et al., 2009	same as SHT17-3
YX07-4	$^{40}Ar/^{39}Ar$ SCLF	sanidine	124.9 ± 1.2	Chang et al., 2009	same as SHT17-3
YL31	U-Pb MAT-216	zircon	125.2 ± 0.9	Wang et al., 2001b	same as SHT17-3
LX-SHT-12	U-Pb SHRIMP	zircon	124.7 ± 2.7	Yang et al., 2007	same as SHT17-3
CY17-17	U-Pb CA-ID-IRMS	zircon	125.46 ± 0.27	Zhong et al., 2021	same as SHT17-1
SHT20-6	$^{40}Ar/^{39}Ar$ SCLF	sanidine	125.23 ± 0.33	This study	tuff
SHT17-1	$^{40}Ar/^{39}Ar$ SCLF	sanidine	125.37 ± 0.24	This study	tuff
SHT17-3	$^{40}Ar/^{39}Ar$ SCLF	sanidine	125.38 ± 0.24	This study	tuff
SHT17-4	$^{40}Ar/^{39}Ar$ SCLF	sanidine	125.41 ± 0.24	This study	tuff
SHT20-1	$^{40}Ar/^{39}Ar$ SCLF	sanidine	125.57 ± 0.25	This study	tuff
Lava Member					
YX07-2	$^{40}Ar/^{39}Ar$ incremental-heating	groundmass	126.9 ± 0.9	Chang et al., 2009	basalt
YX07-2	$^{40}Ar/^{39}Ar$ incremental-heating	groundmass	127.2 ± 0.9	Chang et al., 2009	basalt
YX07-6	$^{40}Ar/^{39}Ar$ incremental-heating	groundmass	130.56 ± 0.90	Chang et al., 2009	basalt
volcanic rock	$^{40}Ar/^{39}Ar$ incremental-heating	groundmass	125.7 ± 2.6	Zhu et al., 2007	basalt
SYNU-005	$^{40}Ar/^{39}Ar$ incremental-heating	groundmass	125.4 ± 1.1	Chang et al., 2017	basalt,
SYNU-010	$^{40}Ar/^{39}Ar$ incremental-heating	groundmass	125.6 ± 0.9	Chang et al., 2017	basalt
YL29	$^{40}Ar/^{39}Ar$ incremental-heating	groundmass	128.4 ± 1.4	Wang et al., 2001a,b	andesite
Lujiatun fossil bed					
L3004	$^{40}Ar/^{39}Ar$ incremental-heating	k-feldspar	124.1 ± 1.5	He et al., 2006	tuff
L3003	$^{40}Ar/^{39}Ar$ incremental-heating	k-feldspar	124.3 ± 1.7	He et al., 2006	tuff
LX-HBJ-1	U-Pb SHRIMP	zircon	124.9 ± 1.7	Yang et al., 2007	tuff
CY17-18	U-Pb CA-ID-IRMS	zircon	125.68 ± 0.27	Zhong et al., 2021	same as LJT17-1
CY17-9	U-Pb CA-ID-IRMS	zircon	125.76 ± 0.27	Zhong et al., 2021	same as LJT17-2
LJT17-1	$^{40}Ar/^{39}Ar$ SCLF	sanidine	125.54 ± 0.25	This study	tuff
LJT17-2	$^{40}Ar/^{39}Ar$ SCLF	sanidine	125.79 ± 0.26	This study	tuff

Notes: The original $^{40}Ar/^{39}Ar$ ages of published references are corrected to decay constants of Min et al. (2000) and 28.201 Ma Fish Canyon Tuff sanidine standard (Kuiper et al., 2008). ± $2\sigma_{ext}$: external uncertainty, fully propagated uncertainty at the 95% confidence interval including analytical, J value, standard age, and decay constant contributions. SCLF: single crystal fusion; CA-ID-IRMS: chemical abrasion-isotope dilution-isotope ratio mass spectrometry.

corporation of older xenocrysts or antecrysts, or reworking of surficial materials into the tuffs. Moreover, the previous $^{40}Ar/^{39}Ar$ dates were generated using single-collector mass spectrometers, and thus are less precise than those obtained using modern multi-collector instruments. For instance, using $^{40}Ar/^{39}Ar$ multi-grain K-feldspar incremental-heating methods, He et al. (2006) determined

ages of 124.3 ± 1.7 and 124.1 ± 1.5 Ma for the Lujiatun fossil bed, and combined these with the age of 125.4 ± 0.8 Ma for Jianshangou fossil bed of Swisher et al. (1999, 2002), to suggest that the Lujiatun fossil bed was deposited contemporaneously with the Jianshangou fossil bed. Chang et al. (2017) report $^{40}Ar/^{39}Ar$ incremental-heating ages of 125.6 ± 0.9 and 125.4 ± 1.1 Ma for the lava horizon that is immediately above the contact with the Lujiatun fossil bed, also indicating that Lujiatun fossil bed was deposited contemporaneously with the Jianshangou fossil bed. However, data from He et al. (2006) and Chang et al. (2017) conflict with the stratigraphic columns from the outcrops and drill cores that suggest the Lujiatun fossil bed is older than the Jianshangou fossil bed (Wang and Zhou, 2003; Wang et al., 2016). Given the uncertainties associated with these earlier age determinations, it has not been possible to resolve the stratigraphic correlation of the two beds.

U-Pb dating of zircon from these tuffs has employed either *in situ* sensitive high resolution ion microprobe (SHRIMP) or chemical abrasion-isotope dilution-isotope ratio mass spectrometry (CA-ID-IRMS) methods. The SHRIMP *in-situ* technique offers rapid, but lower age precision (±2%) determination, whereas the CA-ID-IRMS technique involves chemical abrasion of entire crystals to overcome Pb loss, and isotopic measurement of Pb and U using thermal ionization mass spectrometry (TIMS), and multi-collection inductively-coupled plasma mass spectrometry (MC-ICP-MS), respectively (Zhong et al., 2021). The latter method can yield U-Pb dates with precisions of ~±0.1%. Note that CA-ID-IRMS differs from the more commonly employed CA-ID-TIMS method (e.g., Mattinson, 2005), in which both U and Pb are measured by TIMS. Recently, Zhong et al. (2021) report two U-Pb CA-ID-IRMS zircon ages of 125.684 ± 0.060(0.072)[0.270] and 125.755 ± 0.061(0.072)[0.270] Ma for the Lujiatun fossil bed and an age of 125.457 ± 0.051(0.064)[0.270] Ma for Jianshangou fossil bed. Zhong et al. (2021) conclude that the Jianshangou fossil bed was deposited after the Lujiatun fossil bed. However, the above isotopic ages span only a portion of the stratigraphic sections, rendering correlation of the two fossil beds uncertain.

It is important to note that the analytical uncertainties of Zhong et al. (2021) are smaller than those of our new $^{40}Ar/^{39}Ar$ for the Lujiatun Formation. However, when the full external uncertainties are considered, the $^{40}Ar/^{39}Ar$ ages are more precise than the U-Pb CA-ID-IRMS ages in Zhong et al. (2021). There are several reasons for this: (1) The astronomically calibrated FCs age of 28.201 ± 0.046 Ma (Kuiper et al., 2008) reduces the total uncertainty of the $^{40}Ar/^{39}Ar$ method to ~0.25%, and (2) Zhong et al. (2021) use the ^{238}U decay constant from Villa et al. (2016), that has a larger uncertainty than in Jaffey et al. (1971) which is used by many U-Pb CA-ID-TIMS labs.

The new $^{40}Ar/^{39}Ar$ findings (Table 1), in particular the 125.572 ± 0.058(0.120)[0.254] Ma age for sample SHT20-1, that is indistinguishable from the age of 125.541 ± 0.071(0.099)[0.246] Ma for LJT17-1, lead us to conclude that the lower part of Jianshangou fossil bed was deposited nearly contemporaneously with the Lujiatun fossil bed. Because abundant fossil-bearing layers are well-preserved between SHT17-4 and SHT20-1, including the main feathered dinosaurs and primitive birds horizon at ~0.2 to 0.9 m above SHT20-1, we propose that the inferred mass mortality events involving dinosaurs occurred rapidly over a period of about 100 kyr or less given the dating uncertainties.

5.2. Implication for the geomagnetic polarity of Barremian strata

Pan et al. (2001) and Zhu et al. (2007) report a normal magnetic polarity for the entire 11 m fossil-bearing succession in the Jianshangou fossil bed (Fig. 4), and combined with $^{40}Ar/^{39}Ar$ ages of 125.7 ± 2.6 and 124.2 ± 2.5 Ma (ages are not reported relative to a standard/fluence monitor) from the underlying and overlying volcanic rock, propose that the entire lacustrine interval was deposited within marine magnetic anomaly M3n of Gradstein et al. (1994). The four precise $^{40}Ar/^{39}Ar$ ages between 125.374 ± 0.085 and 125.572 ± 0.120 Ma (ignoring SHT20-6) are within sedimentary rocks possessing normal magnetic polarity (Fig. 4). However, in GTS 2020 (Gale et al., 2020; Ogg, 2020) the period corresponding to these age determinations occurs during marine magnetic anomaly M3r with reversed polarity from 126.5 to 124.7 Ma (Fig. 4). Thus, either the normal polarity chron M3n within the Barremian stage began earlier and lasted longer, or the top of M5n may be younger than inferred in GTS 2020 (Gale et al., 2020). This likely reflects uncertainty in the spline-fit age model of Gale et al. (2020) for the Barremian stage.

5.3. Duration and depositional rate of the Jianshangou fossil bed

Our $^{40}Ar/^{39}Ar$ ages, combined with an astrochronologic age model from bed 6 (Wu et al., 2013), allow for refining the duration of the Jianshangou fossil bed that preserves primitive birds and feathered dinosaurs. Time series analysis of magnetic properties including anhysteretic remanent magnetization (ARM) and magnetic susceptibility (MS) of bed 6 reveals periodicity that may correspond with orbitally-paced short eccentricity, obliquity, and precession cycles (Wu et al., 2013). ARM cycles preserved as ~1.1 to 2.6 m thick intervals of sediment are interpreted by Wu et al. (2013) to reflect pacing by ~100 kyr short eccentricity. Alternatively, based on time series analysis of color and lamination indices of cores drilled from the lacustrine section, these ~1.1 to 2.6 m cycles have been interpreted by Wang et al. (2016) to reflect either ~20 kyr precessional, or ~37 kyr obliquity cycles. However, it is impossible to determine which interpretation is correct from these observations alone without high-resolution radioisotopic age constraints.

We integrate five $^{40}Ar/^{39}Ar$ age determinations with the astronomical age model of Wu et al. (2013) and consider three possible scenarios: First, the $^{40}Ar/^{39}Ar$ ages from tuffs SHT17-1, SHT17-3 and SHT17-4 are indistinguishable from one another, and together indicate that all three could have been deposited over a period of no more than about 100 kyr, centered at 125.39 Ma (the internal uncertainty when comparing among only $^{40}Ar/^{39}Ar$ dates is ± 50 kyr). This can be used to anchor the astronomical age model of Wu et al. (2013). Noting that these three tuffs span 2.4 m of the 11 m thick Jianshangou lacustrine sediment bed (Fig. 4), a sedimentation rate of 2.4 cm/kyr is implied. If the sedimentation rate was constant, this further implies that the entire 11 m section preserves about 460 kyr of time. This interpretation is consistent with the ARM cycles recording short eccentricity. Second, if the ages of the SHT17-1 and SHT17-4 are taken at face value (ignoring the uncertainties), the 2.4 m interval of sediment corresponds to only 40 kyr of time and the sedimentation rate is 6 cm/kyr, which is more consistent with 20 kyr cyclicity paced by precession. Third, the duration between SHT17-1 and SHT20-1 is 198 ± 77 kyr (taking into account the analytical uncertainties), so the 4.6 m interval of sediment corresponds to a deposition rate of 2.32 cm/kyr with range of 1.78 to 3.8 cm/kyr, which is consistent with the ARM cycles recording short eccentricity. The age determined from tuff SHT20-6, despite comprising only two of 76 crystals measured, also implies a sedimentation rate of 1.85 cm/kyr, thereby supporting pacing of cycles by ~100 kyr short eccentricity.

Both the first and third scenarios above correspond to a sedimentation rate of 1.8-2.4 cm/kyr, and support the hypothesis that the ARM variations reflect short eccentricity cycles. The third scenario gives a robust determination for sedimentation rate and duration using the dates of SHT17-1 and SHT20-1. Therefore, we infer that the periodic behavior of magnetic properties in the 11 m of

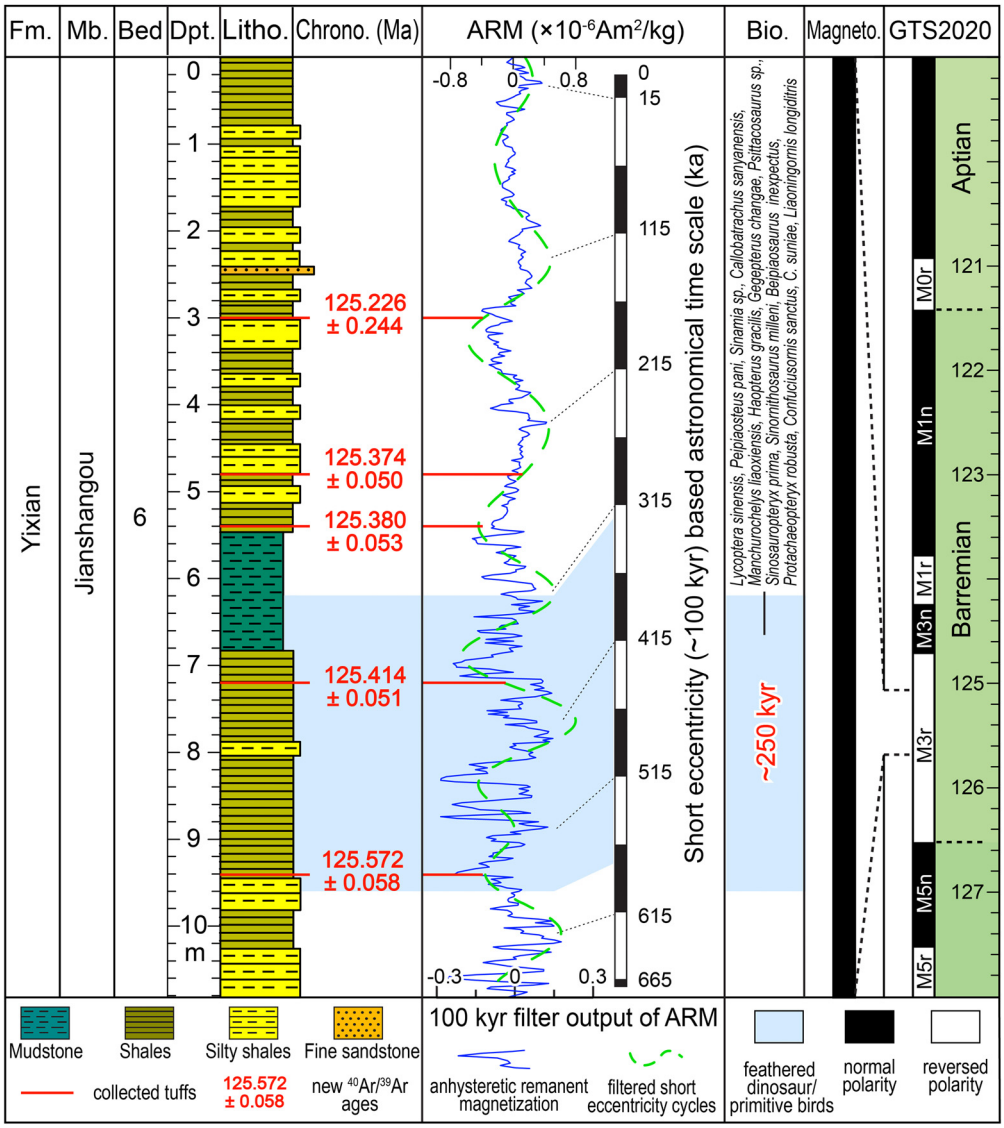

Fig. 4. Integration of lithostratigraphy, radioisotopic chronology, astrochronology, biostratigraphy, and magnetostratigraphy from Bed 6 of Jianshangou Member on the Sihetun section. The red lines and numbers represent tuffs and new $^{40}Ar/^{39}Ar$ ages reported here, from top to bottom: SHT20-6, SHT17-1, SHT17-3, SHT17-4, and SHT20-1. Lithostratigraphy and astrochronology are modified from Wu et al. (2013). Fm—Formation; Mb—Member; Dpt—Depth; Litho—Lithology; Chrono—Chronology; Bio—Biostratigraphy; Magneto—Magnetostratigphy; GTS2020—Geological time scale 2020 modified from Gale et al., 2020; Ogg, 2020. (For interpretation of the colors in the figure(s), the reader is referred to the web version of this article.)

lacustrine strata that preserve primitive birds and feathered dinosaurs in the Jianshangou fossil bed reflect modulation by short eccentricity, rather than obliquity or precession (Fig. 4). Assuming a constant sedimentation rate, the duration of the entire 11 m lacustrine sequence is ~460 to 610 kyr, consistent with the 660 kyr duration proposed by Wu et al. (2013). Moreover, the main fossil-bearing horizon between 6.2 and 9.6 m depth in the section may span as little as ~250 kyr (Fig. 4).

5.4. Rapid preservation and radiation of Jehol Biota in the lower Yixian Formation

The radiation of the Jehol Biota has been divided into early, middle, late stages (Chen, 1988; Zhou, 2006). The middle stage, best recorded in the lower Yixian Formation in the western part of Liaoning Province, was likely the most vibrant as evinced by the greatest species diversification (Chen, 1988; Wang et al., 1998, 2020; Zhou, 2006). The Jianshangou fossil bed has exceptionally well preserved feathered dinosaurs, including *Sinosauropteryx prima, Sinornithosaurus milleni, Beipiaosaurus inexpectus*, *Protachaeopteryx robusta, Caudipteryx zoui and C. dongi* and ceratopsian dinosaur *Psittacosaurus*; primitive birds, *Confuciusornis sanctus, C. suniae, Liaoningornis longiditris*; Pterosaurs, *Haopterus gracilis, Gegepterus changae, Eosipterus yangi, Dendrorhynchoides curvidentatus* (Wang et al., 1998; Wang and Zhou, 2003; Jiang and Sha, 2007). Additionally, this bed is also rich in primitive mammals, fishes, insects, ostracods, gastropods, bivalves, and plants (e.g., angiosperm *Archaefructus liaoningensis*). Therefore, the Jianshangou fossil bed not only contains a large number of new genera and species, but also the total number of individual fossil specimens is abundant. For instance, the density for primitive bird *Confuciusornis sanctus* is average 1 fossil per 2-3 m^2 in the 0.5 mm thick shale at the Sihetun locality (e.g., Wang et al., 1998). Therefore, the short duration of ~460 to 610 kyr of the entire 11 m sequence records abundant new genera and species, that could reflect a very rapid faunal radiation coupled with a high rate of preservation in the Jianshangou fossil bed. Moreover, the feathered dinosaurs and primitive birds died simultaneously, together with aquatic animals (abundant fish, choristoderes), and all of this is mainly preserved within 3.4 m of sediment (Wang et al., 1998) which may span as

little as ~250 kyr based on the new $^{40}Ar/^{39}Ar$ results reported here (Fig. 4). The short duration of ~250 kyr permits exceptional preservation of soft tissues and microstructures (Zhou et al., 2003; Zhang et al., 2010), which is unusual. Volcanic eruptions have often been invoked to explain the mass mortality and exceptional preservation of the Jehol fossils (e.g., Guo et al., 2003; Wang et al., 2020). Volcanism likely triggered forest fires that emitted toxic gases, forcing the terrestrial animals to crowd the lake for safety. Following death, the poisoned or drowned bodies floated in the lake, and were rapidly buried by numerous ash fall deposits (e.g., Guo et al., 2003; Wang et al., 2020).

The Lujiatun fossil bed shows exceptionally high-quality preservation of three-dimensional and articulated fossils. For instance, troodontid dinosaur *Mei long* with sleeping (or resting) posture; ceratopsian dinosaur *Psittacosaurus* with post-nestling gregarious social behavior and an adult *Psittacosaurus* clustering with 34 juveniles; oviraptorosaurian dinosaur *Incisivosaurus gauthieri* displaying distinct dental adaptations for an herbivorous diet; troodontid dinosaur *Sinovenator changii* improving our understanding of the transition of several salient osteological characters to birds; ceratopsian dinosaur *Liaoceratops yanzigouensi*, the most basal neoceratopsian; *Jeholosaurus shangyuanensis*, an ornithopod; *Graciliraptor lujiatunensis*, a dromaeosaurid, *Sinucerasaurus magnodens*, another troodontid, and *Dilong paradoxus*, a basal tyrannosaurid (e.g., Xu et al., 2002; Xu and Norell, 2004; Meng et al., 2004; Zhao et al., 2007). In addition, anuran, lizards and mammals were also discovered in the Lujiatun fossil bed, but flying primitive birds and Pterosaurs are lacking. The Lujiatun fossil bed comprises fluvial and alluvial volcanic-rich conglomerates, tuffaceous sandstones, and tuffs that are structureless, massive and lack bedding planes. It is commonly suggested the vertebrates were killed and buried by pyroclastic flows along the basin margin (Wang and Zhou, 2003; Zhao et al., 2007; Jiang et al., 2014). The new $^{40}Ar/^{39}Ar$ ages indicate that the Lujiatun fossil bed and the lower part of Jianshangou fossil bed formed over a period of about 100 kyr or less given the dating uncertainties. Therefore, these are the most direct radioisotopic findings supporting the idea that the lower Yixian Formation records the most diverse dinosaur assemblage (carnivorous and herbivorous) and the rapid preservation of a dinosaur assemblage that records an important radiation. The brief duration of these faunal records offers new ways to interpret the nature of the mass mortality event and preservation mechanisms.

6. Conclusions

Single crystal $^{40}Ar/^{39}Ar$ sanidine dates from seven tuffs constrain the deposition of the two well-preserved fossil-bearing Jianshangou and Lujiatun fossil beds to between 125.374 ± 0.085 and 125.572 ± 0.120 Ma, and 125.541 ± 0.099 and 125.793 ± 0.127 Ma, respectively. The new $^{40}Ar/^{39}Ar$ dates span more of the salient stratigraphic sections than previous investigations, and suggest that the lower part of Jianshangou fossil bed was deposited nearly contemporaneously with the Lujiatun fossil bed. Combining these ages with astrochronologic results for Jianshangou fossil bed, we propose that the 11 m of lacustrine strata preserving primitive birds and feathered dinosaurs reflect modulation by ~100 kyr orbital eccentricity cycles, and that the duration of the biological radiations recorded within this sequence is only ~460 to 610 kyr. Moreover, linked to paleomagnetic results, our findings indicate that the normal polarity chron M3n within the Barremian stage either begins earlier, or the top of chron M5n may be younger, than expressed in the current geologic time scale (GTS 2020).

CRediT authorship contribution statement

Youjuan Li: Conceptualization, Investigation, Methodology, Visualization, Writing – original draft. **Brian R. Jicha:** Investigation, Methodology, Resources, Writing – review & editing. **Zhiqiang Yu:** Resources, Writing – review & editing. **Huaichun Wu:** Resources, Writing – review & editing. **Xiaolin Wang:** Writing – review & editing. **Brad S. Singer:** Funding acquisition, Methodology, Supervision, Writing – review & editing. **Huaiyu He:** Funding acquisition, Methodology, Project administration, Supervision, Writing – review & editing. **Zhonghe Zhou:** Funding acquisition, Writing – review & editing.

Declaration of competing interest

The authors declare that they have no known competing financial interests or personal relationships that could have appeared to influence the work reported in this paper.

Acknowledgements

We thank Bryan Wathen for his help with sample preparation. We thank two anonymous reviewers and Editor Boswell Wing for their insightful and constructive comments, which helped to improve this paper. This work was supported by the National Natural Science Foundation of China (41688103, 41425013, and 41790451) and the Strategic Priority Research Program B of the Chinese Academy of Sciences (XDB 18030505). The WiscAr Laboratory is supported in part by U.S. NSF grant EAR-1951812.

Appendix A. Supplementary material

Supplementary material related to this article can be found online at https://doi.org/10.1016/j.epsl.2022.117718.

References

Andersen, N.L., Jicha, B.R., Singer, B.S., Hildreth, W., 2017. Incremental heating of Bishop Tuff sanidine reveals preeruptive radiogenic Ar and rapid remobilization from cold storage. Proc. Natl. Acad. Sci. 114, 12407–12412. https://doi.org/10.1073/pnas.1709581114.

Chang, S.C., Zhang, H.C., Renne, P.R., Fang, Y., 2009. High-precision $^{40}Ar/^{39}Ar$ age for the Jehol Biota. Palaeogeogr. Palaeoclimatol. Palaeoecol. 280, 94–104. https://doi.org/10.1016/j.palaeo.2009.06.021.

Chang, S.C., Gao, K.Q., Zhou, C.F., Jourdan, F., 2017. New chronostratigraphic constraints on the Yixian Formation with implications for the Jehol Biota. Palaeogeogr. Palaeoclimatol. Palaeoecol. 487, 399–406. https://doi.org/10.1016/j.palaeo.2017.09.026.

Chen, P.J., 1988. Distribution and migration of the Jehol fauna with reference to the nonmarine Jurassic-Cretaceous boundary in China. Acta Palaeontol. Sin. 27, 659–683 (in Chinese, abstract in English).

Deino, A., Potts, R., 1990. Single-crystal $^{40}Ar/^{39}Ar$ dating of the Olorgesailie Formation, Southern Kenya Rift. J. Geophys. Res. 95 (B6), 8453–8470. https://doi.org/10.1029/JB095iB06p08453.

Ellis, B.S., Mark, D.F., Troch, J., Bachmann, O., Guillong, M., Kent, A.J., von Quadt, A., 2017. Split-grain $^{40}Ar/^{39}Ar$ dating: integrating temporal and geochemical data from crystal cargoes. Chem. Geol. 457, 15–23. https://doi.org/10.1016/j.chemgeo.2017.03.005.

Gale, A.S., Mutterlose, J., Batenburg, S., 2020. The Cretaceous period. In: Gradstein, F.M., Ogg, J.G., Schmitz, M.D., Ogg, G.M. (Eds.), The Geologic Time Scale 2020, vol. 2. Elsevier, pp. 1023–1086.

Gradstein, F.M., Agterberg, F.P., Ogg, J.G., Hardenbol, J., van Veen, P., Thierry, T., Huang, Z., 1994. A Mesozoic time scale. J. Geophys. Res. 99, 24051e24074.

Guo, Z.F., Liu, J.Q., Wang, X.L., 2003. Effects of Mesozoic volcanic eruption on the paleoclimate and paleovertebrate living environment. Sci. China 33, 59–71. https://doi.org/10.3969/j.issn.1000-0569.2002.01.013 (in Chinese, abstract in English).

He, H.Y., Wang, X.L., Zhou, Z.H., Jin, F., Wang, F., Yang, L.K., Ding, X., Boven, A., Zhu, R.X., 2006. $^{40}Ar/^{39}Ar$ dating of Lujiatun bed (Jehol Group) in Liaoning, northeastern, China. Geophys. Res. Lett. 33. https://doi.org/10.1029/2005GL025274.

Hu, Y.M., Meng, J., Wang, Y.Q., Li, C.K., 2005. Large Mesozoic mammals fed on young dinosaurs. Nature 433, 149–152. https://doi.org/10.1038/nature03102.

Jaffey, A., Flynn, K., Glendenin, L., Bentley, W.T., Essling, A., 1971. Precision measurement of half-lives and specific activities of ^{235}U and ^{238}U. Phys. Rev. C 4, 1889. https://doi.org/10.1103/PhysRevC.4.1889.

Jiang, B.Y., Sha, J., 2007. Preliminary analysis of the depositional environments of the Lower Cretaceous Yixian Formation in the Sihetun area, western Liaoning, China. Cretac. Res. 28, 183–193. https://doi.org/10.1016/j.cretres.2006.05.010.

Jiang, B.Y., Harlow, G.E., Wohletz, K., Zhou, Z., Meng, J., 2014. New evidence suggests pyroclastic flows are responsible for the remarkable preservation of the Jehol Biota. Nat. Commun. 5, 1–7. https://doi.org/10.1038/ncomms4151.

Jicha, B.R., Singer, B.S., Sobol, P., 2016. Re-evaluation of the ages of ^{40}Ar/^{39}Ar sanidine standards and supereruptions in the western US using a Noblesse multi-collector mass spectrometer. Chem. Geol. 431, 54–66. https://doi.org/10.1016/j.chemgeo.2016.03.024.

Kuiper, K.F., Deino, A., Hilgen, F.J., Krijgsman, W., Renne, P.R., Wijbrans, J.R., 2008. Synchronizing rock clocks of Earth history. Science 320, 500–504. https://doi.org/10.1126/science.1154339.

Lee, J.Y., Marti, K., Severinghaus, J.P., Kawamura, K., Yoo, H.S., Lee, J.B., Kim, J.S., 2006. A redetermination of the isotopic abundances of atmospheric Ar. Geochim. Cosmochim. Acta 70, 4507–4512. https://doi.org/10.1016/j.gca.2006.06.1563.

Leng, Q., Friis, E.M., 2003. Sinocarpus decussatus gen. et sp. nov., a new angiosperm with basally syncarpous fruits from the Yixian Formation of Northeast China. Plant Syst. Evol. 241, 77–88. https://doi.org/10.1007/s00606-003-0028-8.

Luo, Z.X., Ji, Q., Wible, J.R., Yuan, C.X., 2003. An early Cretaceous tribosphenic mammal and metatherian evolution. Science 302, 1934–1940. https://doi.org/10.1126/science.1090718.

Manabe, M., Barrett, P.M., Isaji, S., 2000. A refugium for relicts. Nature 404, 953. https://doi.org/10.1038/35010199.

Mattinson, J.M., 2005. Zircon U–Pb chemical abrasion ("CA-TIMS") method: combined annealing and multi-step partial dissolution analysis for improved precision and accuracy of zircon ages. Chem. Geol. 220, 47–66. https://doi.org/10.1016/j.chemgeo.2005.03.011.

Meng, Q.J., Liu, J.Y., Varricchio, D.J., Huang, T., Gao, C.L., 2004. Parental care in an ornithischian dinosaur. Nature 431, 145–146. https://doi.org/10.1038/431145a.

Min, K., Mundil, R., Renne, P.R., Ludwig, K.R., 2000. A test for systematic errors in ^{40}Ar/^{39}Ar geochronology through comparison with U/Pb analysis of a: 1.1-Ga Rhyolite. Geochim. Cosmochim. Acta 64, 73–98. https://doi.org/10.1016/S0016-7037(99)00204-5.

Ogg, J.G., 2020. Geomagnetic polarity time scale. In: Gradstein, F.M., Ogg, J.G., Schmitz, M.D., Ogg, G.M. (Eds.), The Geologic Time Scale 2020, vol. 1. Elsevier, pp. 159–192.

Pan, Y.X., Zhu, R.X., John, S., Zhou, Y.X., 2001. Magnetic polarity ages of the fossil-bearing strata at the Sihetun section, West Liaoning: a preliminary result. Chin. Sci. Bull. 46, 1473–1476. https://doi.org/10.1007/BF03187035.

Rogers, C.S., Hone, D.W., McNamara, M.E., Zhao, Q., Orr, P.J., Kearns, S.L., Benton, M.J., 2015. The Chinese Pompeii? Death and destruction of dinosaurs in the early Cretaceous of Lujiatun, NE China. Palaeogeogr. Palaeoclimatol. Palaeoecol. 427, 89–99. https://doi.org/10.1016/j.palaeo.2015.03.037.

Ross, J., 2019. NMGRL/pychron, v18.2. https://doi.org/10.5281/zenodo.3237834.

Schaen, A.J., Jicha, B.R., Hodges, K.V., et al., 2021. Interpreting and reporting ^{40}Ar/^{39}Ar geochronologic data. Geol. Soc. Am. Bull. 133, 461–487. https://doi.org/10.1130/B35560.1.

Swisher, C.C., Wang, Y.Q., Wang, X.L., Xu, X., Wang, Y., 1999. Cretaceous age for the feathered dinosaurs of Liaoning, China. Nature 400, 58–61. https://doi.org/10.1038/21872.

Swisher, C.C., Wang, X.L., Zhou, Z.H., Wang, Y.Q., Jin, F., Zhang, J.Y., Xu, X., Zhang, F.C., Wang, Y., 2002. Further support for a Cretaceous age for the feathered-dinosaur beds of Liaoning, China. New ^{40}Ar/^{39}Ar dating of the Yixian and Tuchengzi Formations. Chin. Sci. Bull. 47, 136–139. https://doi.org/10.1360/02tb9031.

Villa, I.M., Bonardi, M.L., De Bièvre, P., Holden, N.E., Renne, P.R., 2016. IUPAC-IUGS status report on the half-lives of ^{238}U, ^{235}U and ^{234}U. Geochim. Cosmochim. Acta 172, 387–392. https://doi.org/10.1016/j.gca.2015.10.011.

Wang, S.S., Wang, Y.Q., He, H.G., Li, H.M., 2001a. The existing time of Sihetun vertebrate in western Liaoning - evidence from U–Pb dating of zircon. Chin. Sci. Bull. 46, 779–782. https://doi.org/10.3321/j.issn:0023-074X.2001.04.014 (in Chinese, abstract in English).

Wang, S.S., Hu, H.G., Li, P.X., Wang, Y.Q., 2001b. Further discussion on the geologic age of the Sihetun vertebrate assemblage in western Liaoning, China. Evidence from Ar-Ar dating. Acta Petrol. Sin. 17, 663e668. https://doi.org/10.3969/j.issn.1000-0569.2001.04.018 (in Chinese, English abstract).

Wang, X.L., Wang, Y.Q., Wang, Y., Xu, X., Tang, Z.L., Zhang, F.H., Hu, Y.M., 1998. Stratigraphic sequence and vertebrate-bearing beds of the lower part of the Yixian Formation, in Sihetun and neighboring area, western Liaoning, China. Vertebr. PalAsiattica. 36, 81–101 (in Chinese, abstract in English).

Wang, X.L., Zhou, Z.H., 2003. Mesozoic Pompeii. In: Chang, M.M., Chen, P.J., Wang, Y.Q., Wang, Y. (Eds.), The Jehol Biota: The Emergence of Feathered Dinosaurs, Beaked Birds and Flowering Plants. Shanghai Scientific & Technical Publishers, Shanghai, pp. 19–36.

Wang, X.L., Li, Y., Qiu, R., Jiang, S.X., Zhang, X.J., Chen, H., Wang, J.X., Cheng, X., 2020. Comparison of biodiversity of the Early Cretaceous pterosaur faunas of China. Earth Sci. Front. 27, 347–364. https://doi.org/10.13745/j.esf.sf.2020.6.19 (in Chinese, abstract in English).

Wang, Y.Q., Olsen, P.E., Sha, J.G., Yao, X.G., Liao, H.Y., Pan, Y.H., Kinney, S., Zhang, X.L., Rao, X., 2016. Stratigraphy, correlation, depositional environments, and cyclicity of the Early Cretaceous Yixian and Jurassic-Cretaceous Tuchengzi formations in the Sihetun area (NE China) based on three continuous cores. Palaeogeogr. Palaeoclimatol. Palaeoecol. 464, 110–133. https://doi.org/10.1016/j.palaeo.2016.06.043.

Wu, H.C., Zhang, S.H., Jiang, G.Q., Yang, T.S., Guo, J.H., Li, H.Y., 2013. Astrochronology for the Early Cretaceous Jehol Biota in Northeastern China. Palaeogeogr. Palaeoclimatol. Palaeoecol. 385, 221–228. https://doi.org/10.1016/j.palaeo.2013.05.017.

Xu, X., Cheng, Y.N., Wang, X.L., Chang, C.H., 2002. An unusual oviraptorosaurian dinosaur from China. Nature 419, 291–293. https://doi.org/10.1038/nature00966.

Xu, X., Norell, M.A., 2004. A new troodontid dinosaur from China with avian-like sleeping posture. Nature 431, 838–841. https://doi.org/10.1038/nature02898.

Yang, W., Li, S., Jiang, B., 2007. New evidence for Cretaceous age of the feathered dinosaurs of Liaoning: zircon U–Pb SHRIMP dating of the Yixian Formation in Sihetun, northeast China. Cretac. Res. 28, 177–182. https://doi.org/10.1016/j.cretres.2006.05.011.

Zhang, F.C., Kearns, S.L., Orr, P.J., Benton, M.J., Zhou, Z., Johnson, D., Xu, X., Wang, X., 2010. Fossilized melanosomes and the colour of Cretaceous dinosaurs and birds. Nature 463, 1075–1078. https://doi.org/10.1038/nature08740.

Zhang, J., Zhang, H., 2003. Insects and spiders. In: Chang, M.M., Chen, P.J., Wang, Y.Q., Wang, Y. (Eds.), The Jehol Biota: The Emergence of Feathered Dinosaurs, Beaked Birds and Flowering Plants. Shanghai Scientific & Technical Publishers, Shanghai, pp. 59–68.

Zhao, Q., Barrett, P.M., Eberth, D.A., 2007. Social behaviour and mass mortality in the basal ceratopsian dinosaur Psittacosaurus (Early Cretaceous, People's Republic of China). Palaeontology 50, 1023–1029. https://doi.org/10.1111/j.1475-4983.2007.00709.x.

Zhong, Y.T., Huyskens, M.H., Yin, Q.Z., Wang, Y.Q., Ma, Q., Xu, Y.G., 2021. High-precision geochronological constraints on the duration of 'Dinosaur Pompeii' and the Yixian Formation. Nat. Sci. Rev. 8 (6), nwab063. https://doi.org/10.1093/nsr/nwab063.

Zhou, Z.H., Barrett, P.M., Hilton, J., 2003. An exceptionally preserved Lower Cretaceous ecosystem. Nature 421, 807–814. https://doi.org/10.1038/nature01420.

Zhou, Z.H., 2006. Evolutionary radiation of the Jehol Biota: chronological and ecological perspectives. Geol. J. 41, 377–393. https://doi.org/10.1002/gj.1045.

Zhou, Z.H., Wang, Y., 2017. Vertebrate assemblages of the Jurassic Yanliao Biota and the early Cretaceous Jehol Biota: comparisons and implications. Palaeoworld 26, 241–252. https://doi.org/10.1016/j.palwor.2017.01.002.

Zhu, R.X., Pan, Y.X., Shi, R.P., Liu, Q.S., Li, D.M., 2007. Palaeomagnetic and ^{40}Ar/^{39}Ar dating constraints on the age of the Jehol Biota and the duration of deposition of the Sihetun fossil-bearing lake sediments, northeast China. Cretac. Res. 28, 171–176. https://doi.org/10.1016/j.cretres.2006.06.003.